Turkish Online Journal of Qualitative Inquiry (TOJQI)
Volume 12, Issue 9, August 2021: 1822-1835

Magneto Optical and Structural Properties of Ni, Ca, and Fe Doped ZnO Nanoparticles by Single-Step Method

Mohamed Haroon Basha A[*1], Steffi PF[2] , Sangeetha K[2] , Bhuvaneswari P[2], Thamilmaraiselvi B[2], Mishel PF[3]

[1]Department of Physics, AMET DEEMED to be University, Chennai, India

[2]PG and Research Department of Microbiology, Cauvery College for Women

(Autonomous), Trichirappalli.

[3]Research scholar, Department of Botany, Bharathidasan University, Trichy.

[*]Corresponding author : harunbasha09@gmail.com

Abstract

Nanostructures of metal oxides are used for determining the optical, electrical and magnetic properties. In this Research work, Composites of nano structured Zno were prepared and their optical and magnetic properties are determined. The prepared composites are composed of ZnNiCaFeO using Co precipitation method. Bare Zno are also prepared to distinguish the role of nano composites and their properties are compared with the composite materials. ZnNiCaFeO exhibited hexagonal wurtzite structure with the grain size about 54nm and 44 nm respectively.From the FESEM and EDAX analysis, Hexagonal nanorod structured morphology and the atomic percentage of the prepared composites are obtained.UV-Vis absorption spectra showed the absorption peak at 298nm for Zno and 288 nm for ZnNiCaFeONPs. Excitation wavelength of the composite materials are obtained from the PL studies. The significant magnetization values of 0.32914 emu/g. of composite ZnNiCaFeO are exhibited with ferromagnetic behavior. The results indicated the composites can be used in soft magnetic application as in various optical applications..

Keywords: Zinc Oxide; Co-precipitation; Wurtzite; Optical properties; Ferromagnetic.

1 Introduction

Multifunctional semiconducting metal oxide ie., Zinc oxide (ZnO) have a direct energy band gap of 3.36 eV and high binding energy of ZNO is 60 meV. Therefore it is used enormous applications in various fields such as magnetic, piezoelectric, optical, photocatalysts, gas sensing and etc., [1,2]. The polar nature of hexagonal wurtzite lattice permitted to grow several nano sized morphologies such as rods, wires, spindle, belts, stars and flowers and etc., by simply controlling the synthesis conditions[3]. Nanocrystalline semiconductors and its optical properties were investigated. due to its strange characteristics such as size and large band gap. Currently, a widespread research has been carried out

to explore the effect of doping various metal elements such as Ni^{2+}, $Co^{2+/3+}$ and $Fe^{2+/3+}$ for modifying the electrical, optical and magnetic properties of various metal oxides [4]. magnetic ferrites ($M_xFe_{3-x}O_4$, where M=Fe, Co, Mn, Ni, or Zn) are versatile nanomaterials these are having super-paramagnetism and tuneable surface properties [5] 3. The optical properties of ferrite systems can also be altered due to the doping process [6]. The ferrite Zn and Ni doping due to the attribution of defects improve the optical and magnetic properties. For the synthesis of pure and doped ZnO NPs, the chemical or physical methods such as solvothermal method and co-precipitation method [7-9] and sol-gel method.The plenty of methods have been reported.the co-precipitation method is one of the versatile simple method which is cost effect, giving high yield and homogeneous mixture of reagent precipitates. In addition, it is a simple technique for the synthesis of the size and morphology of the metal oxides and hydroxides.

In this work, the sample ZnO and Ca, Ni and Fe mixed forms to ZnO matrix, such as ZNCFO nanoparticles ($Zn_{0.090}(Ni_{0.05}Ca_{0.05})Fe_{0.010}O$) via co-precipitation method has been synthesised and characterised. As prepared samples were subjected to various characterization such as XRD, FTIR,Photo Luminescence (PL), VSM and etc.,.

2. Materials and methods

Zinc (II) nitrate hexahydrate ($Zn(NO_3)_2.6H_2O$), Nickel (II) nitrate hexahydrate ($Ni(NO_3)_2.6H_2O$), Calcium (II) nitrate tetrahydrate ($Ca(NO_3)_2.6H_2O$, Iron (III) nitrate nonahydrate ($Fe(NO_3)_3.9H_2O$) and Sodium hydroxide (NaOH) were purchased from NICE chemicals and used as received.

2.1 Synthesis of ZnNiCaFeO NPs

The nanopowders of ZnO were well synthesized using previously reported procedures [8]. Briefly, precursor solution of $Zn_{0.090}(Ni_{0.05}Ca_{0.05})Fe_{0.010}O$ NPs (ZnNiCaFeO), was obtained using co-precipitation process in which 90 mmol Zinc nitrate, 50 mmol Nickel nitrate, 50 mmol Calcium nitrate and 10 mmol Iron nitrate were dissolved separately using distilled water as a common solvent. Further all the precursor solutions were mixed together to get homogenous solution and the solution is continuously stirred and 0.8 M of NaOH solution is prepared and added drop wise to the above solution until obtaining the brown colour precipitate. Thereafter, the precipitate powder was washed several times using double distilled water followed by ethanol solvents until reaching the pH of the washed solution to neutral condition. After washing, the collected powder was dried at 120 $^{\circ}$C for 6 h in vacuum oven . The product was calcinated at 700 °C for 6h in a muffle furnace at air medium to get pure ZnO and ZnNiCaFeO samples.

2.2. Characterization techniques

The samples ZnNiCaFeO NPs and ZnO were characterized by X-ray diffractometer and recorded in the range of 25-85^o with the monochromatic wavelength of 1.54 Å. Morphological studies were performed in (Carl Zeiss Ultra 55 FESEM) with EDAX (model: Inca) model. FT-IR spectra of the samples were recorded in the range of 400-4000 cm^{-1} by using Perkin-Elmer spectrophotometer. Using Burker RFS 25 spectrometer, Raman spectra were recorded. The absorption spectra of the samples were carried in the range between 200 and 1100 nm by Lambda 35 spectrometer. The vibrating sample magnetometer were recorded 2.07 Tesla.

3. Results and Discussion

For the ZnO and ZnNiCaFeO NPs samples, the X-ray diffraction patterns are recorded are shown in Fig. 1a.The Characteristic peaks obtained at 3. angle of (2θ) of 30.8, 34.4, 36.2, 47.5, 56.4, 62.8, 66.2, 67.8 and 69.2º are corresponding to (100) (002) (101) (102) (110) (103) (200) (112) and (201) lattice planes of the ZnO NPs.The hexagonal wurtzite structure of ZnO NPs with space group p63mc, which is coordinated with the JCPDS data (Card No: 79-2205) and the samples of standard diffraction peaks are confirmed . For examine the effect of the composite structure of ZnO on ZnNiCaFeO are confirmed from the XRD pattern (Fig. 1b). In case of the sample ZnNiCaFeO NPs, which has emerged an angle between 37and 43.1º corresponding to Fe_3O_4 along (311) and (400) planes [10], further, the unreacted Fe^{3+} present in the final composition is also evidenced from the Fig.1(c-d).

The lattice constant 'a' and the lattice constant 'c' of the wurtzite structure of ZnO NPs is calculated by

$$\frac{1}{d^2} = \frac{4}{3}\left(\frac{h^2+hk+k^2}{a^2}\right) + \frac{l^2}{c^2} \qquad (1)$$

And for the (100) plane with the first order approximation (n = 1). The lattice constant 'a' is obtained through the relation a =$\frac{\lambda}{\sqrt{3}\sin\theta}$ and lattice constant 'c' is derived for the plane (002) by the relation c =$\frac{\lambda}{\sin\theta}$. 5. The estimated values of 'a' and 'c' are 3.4272 and 5.4024 Å for ZnO NPs whereas ZnNiCaFeO The calculated values of 'a' and 'c' are 3.2472 and 5.2024 Å for ZnO NPs whereas ZnNiCaFeO NPs have 3.2282 and 5.1982 Å, respectively (Table 1).

The calculated values showed decrease in lattice constants due to the effect of Fe atoms trapped in the non-equilibrium position are shifted to a more equilibrium position. 6. The lattice parameter of the sample values are given in Table 1.

$$V = \frac{\sqrt{3}a^2c}{2} = 0.866a^2c \qquad (2)$$

The unit cell volumes calculated by the equation (2) which is found to be 47.50 $Å^3$ and 47.4959$Å^3$ for pure ZnO and ZnNiCaFeO NPs, respectively. The effect of doping on bond length of Zn-O is calculated by using the relation,

$$L=\sqrt{\left(\frac{a^3}{3} + \left(\frac{1}{2} - u\right)^2 c^2\right.} \qquad (3)$$

where 'a' and 'c' are lattice parameters and 'u' positional parameter which is measured from the amount by which each atom is displaced with respect to the next along the c-axis. The parameter 'u' can be estimated by the formula

$$u= \left(\frac{a^2}{3c^2}\right) + 0.25 \qquad (4)$$

showed a strong correlation between the c/a ratio and 'u'. The c/a ratio decreases in the ZnNiCaFeO NPs as compared to that of the ZnO NPs is observed in Table 2.

The bond length of pure ZnO sample and the sample ZnNiCaFeO NPs are 1.9757 and 1.9756 Å, respectively, and the change in bond length is attributed to high ionic radius of Fe3 ion. In hexagonal wurtzite structure, the metal ion and the oxygen ion in ZnO sample faces directly placed in "c" axis, but for the "a" and "b" axis, the structure encloses only oxygen facing each other. Oxygen ion is obliquely connected to the metal ion so that the variation is significant in "c" axis only but not in "a" axis [11].

Debye Scherrer's relation [8] calculates the average size of the crystalline sample. The average crystal sizes 50 and 45 nm for ZnO and the sample ZnNiCaFeO NPs, respectively. The particles size reduced due to the distortion in the host ZnO lattice due to the external impurity, i.e. Ni^{2+}, Ca^{2+} and Fe^{3+} ions, decreases the nucleation and consequent growth rate of the sample ZnO NPs.

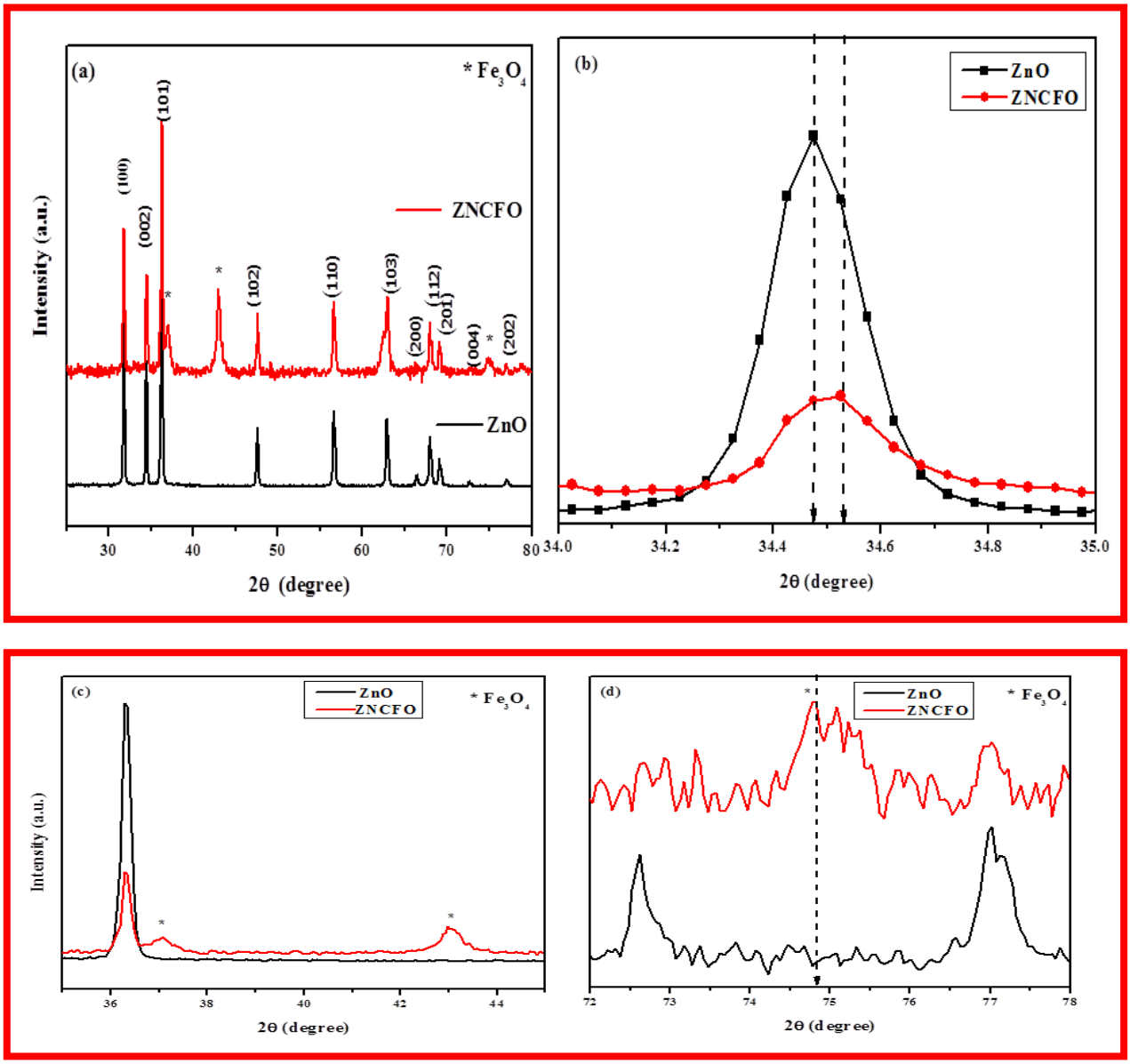

Figure 1. X-Ray diffraction pattern of (a) ZnO and ZNCFO NPs (b) the doping-induced peak shift for NPs (c and d) enhanced XRD spectra of Fe_3O_4 secondary peaks.

Table 1: Lattice parameters, atomic peak factors, bond length of ZnO and ZNCFO NPs

JCPDS Card no: (79-2205) 2θ (degree)	ZnO 2θ (degree)	ZNCFO 2θ (degree)	JCPDS Card no: (79-2205) d-spacing [Å]	ZnO d-spacing [Å]	ZNCFO d-spacing [Å]	ZnO (hkl)	ZNCFO (hkl)	JCPDS Card no: (79-2205) Rel. Int. [%]	ZnO Rel. Int. [%]	ZNCFO Rel. Int. [%]
31.799	31.795	31.784	2.8146	2.81218	2.81309	(100)	(100)	56.40	61.10	50.57
34.419	34.45	34.479	2.6035	2.60123	2.59914	(002)	(002)	41.50	48.83	32.50
36.251	36.278	36.28	2.4760	2.47426	2.47414	(101)	(101)	99.99	100.00	100.00
-	-	37		-	2.4245	-	(222)*	-		11.52
-		43.01			2.10113	-	(400)*	-		24.11
47.536	47.566	47.58	1.9112	1.9101	1.90947	(102)	(102)	21.10	22.07	20.39
56.591	56.617	56.61	1.6250	1.62435	1.62456	(110)	(110)	30.50	33.24	27.01
62.851	62.891	62.93	1.4773	1.47656	1.47571	(103)	(103)	26.80	30.36	21.61
66.371	66.4	-	1.4073	1.40674	-	(200)	-	4.00	4.35	-
67.942	67.979	67.97	1.3785	1.3779	1.37797	(112)	(112)	21.70	20.32	16.43
69.081	69.106	69.1104	1.3585	1.35814	1.3592	(201)	(201)	10.6	11.12	10.70
72.560	72.59	-	1.3017	1.30124	-	(004)	-	1.70	1.96	-
-	-	74.7	-	-	1.26929	-	(622)*	-	-	4.82
76.953	77	76.9	1.2380	1.23745	1.2381	(202)	(202)	3.30	2.76	4.12

***Fe_3O_4 = JCPDS Card No:87-2334**

Table 2: Lattice parameters, atomic peak factors, bond length of ZnO and ZNCFO

Samples	Lattice parameters (Å)		Atomic peak factor c/a	Bond length (L) Å	Cell volume (V) $Å^3$	Average crystalline size (D) nm
	a	C				
ZnO	3.2472	5.2024	1.6021	1.9758	47.5050	52
ZNCFO	3.2282	5.1982	1.6003	1.9756	47.4959	46

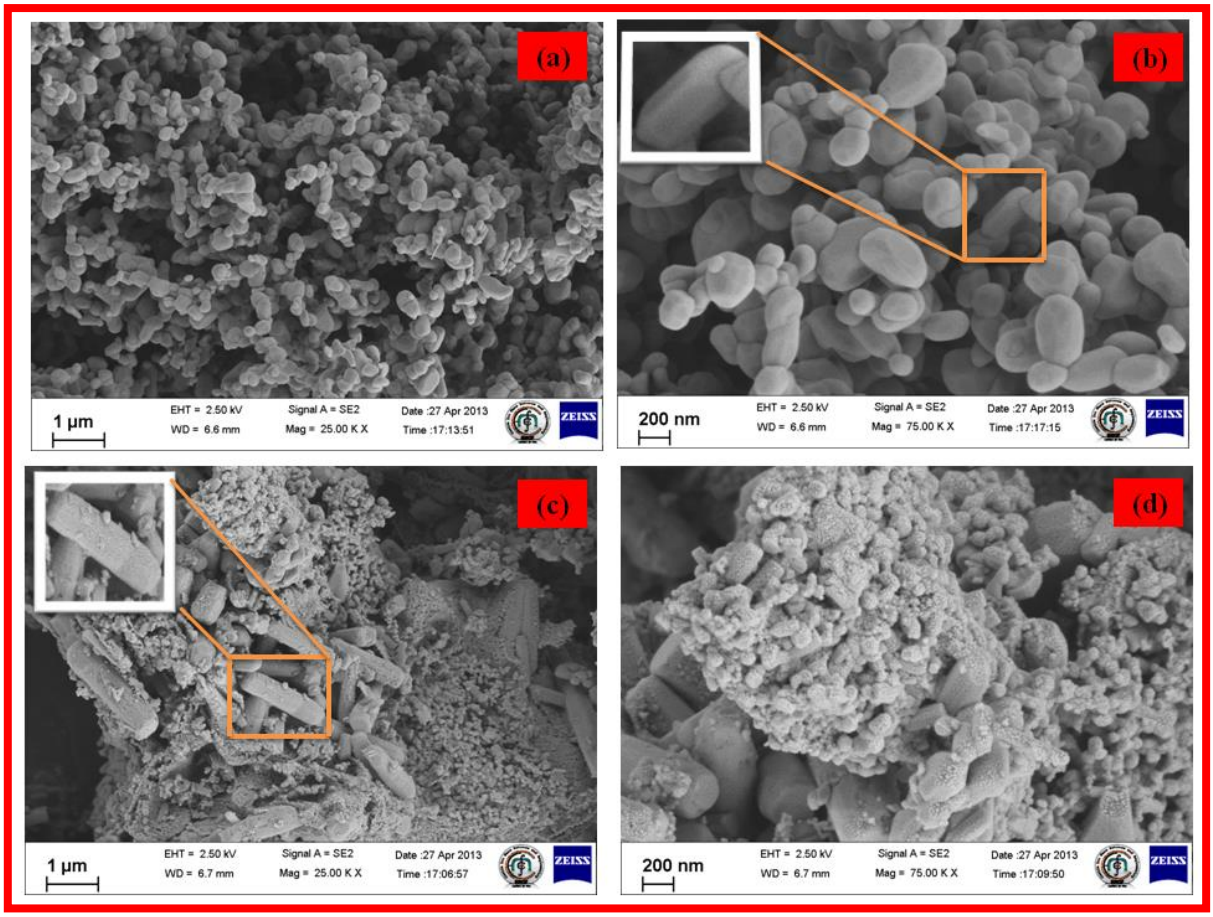

Figure 2. FESEM image with low and high resolution for (a-b) ZnO NPs (c-d) ZNCFO NPs

From FESEM analysis, the surface morphology of the ZnO sample and ZnNiCaFeO NPs are observed at different magnifications. (Fig. 2(a-d)). The FESEM image clearly shows the uniform size of the NPs in the order of nanometer size of below 200. The ZnO NPs are exhibits hexagonal spherical like structure with even grain sizes. 13.The particles in the Nano rod shaped in the sample ZnNiCaFeO composite were overlapped on the hexagonal structured ZNO which is confirmed the presence of the other compounds are also evidenced from the EDAX spectrum. Using EDX spectra the chemical composition analysis of ZnO and ZnNiCaFeO NPs are carried out as shown in Fig.3a and b, respectively.The amounts of Zn, Ni, Ca, Fe and O present in the pure ZnO and ZnNiCaFeO samples are calculated from given values and observed from EDX analysis.In the composite sample, the concentration of Ca , Fe and Ni are found to be 22.18, 22.41 and 2 In the ZnO and ZnNiCaFeO NPs, the chemical composition of Zn and O are found as (52.44% and 47.56%) and (24.69% and 31.80%), respectively which is confirmed the effective compound for the formation during the synthesis process.

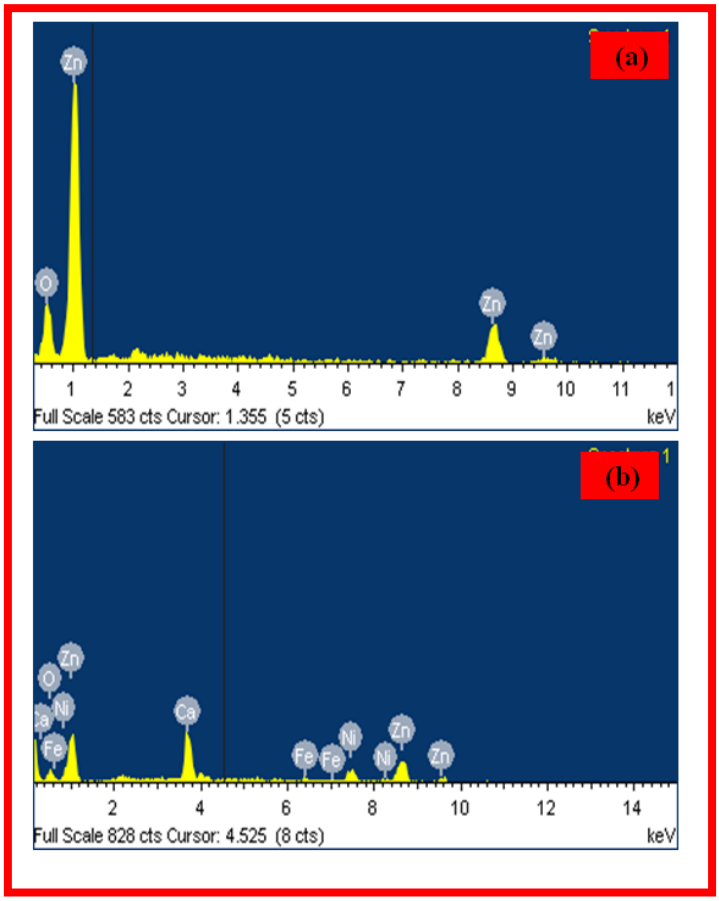

Figure 3: EDX spectra of a) ZnO and b) ZNCFO NPs

Table 3 Elemental composition of ZnO and ZnNiCaFeO **NPs**

Element	Weight%	Atomic%	Element	Weight%	Atomic%
O K	21.25	52.44	O K	11.91	31.82
Zn L	78.75	47.56	Ca K	19.99	21.31
			Fe K	2.64	2.02
Totals	100.00		Ni K	27.70	20.16
			Zn L	37.77	24.69
			Totals	100.00	

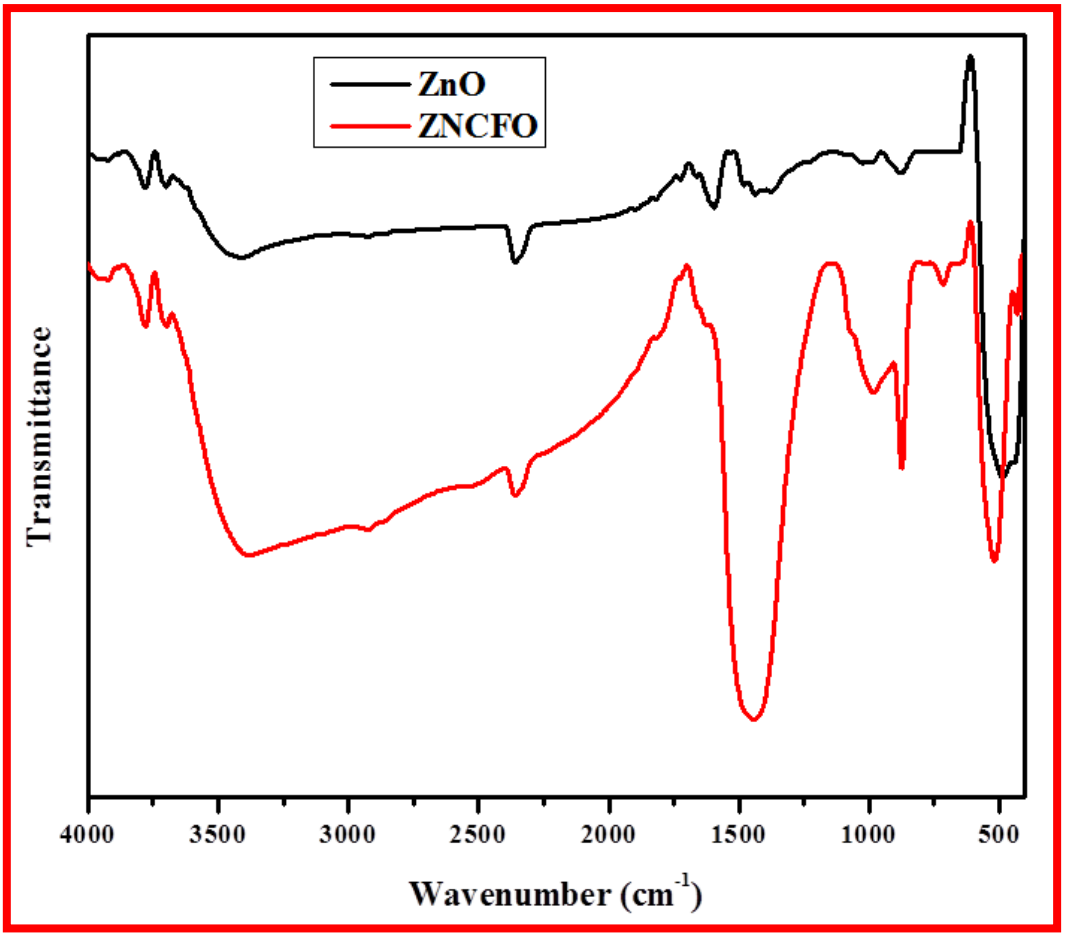

Figure 4 FT-IR Spectra of pure ZnO and ZnNiCaFeO NPs

Further, the b band formation of the composite and the pure ZnO samples are evidenced from the FTIR spectral analysis. Fig. 4 showed FTIR spectra of the ZnO and ZnNiCaFeO samples; the spectra showed the peaks around at 3443 and 3418 cm^{-1} which are corresponding to O-H stretching vibration whereas the peaks at 1633 $cm^{-1}$and 1618 cm^{-1} related to O-H bending vibration [12] of the prepared samples. In the ZnO sample, the Zn-O band was observed at at 445 cm^{-1} [11]. The ZnO band has shifted to 622 cm-1 - 552 cm-1 range in the ZnNiCaFeO composite and the sample has confirmed the presence of stabilized $Ni2^{+}$ and Ca^{2+} in the ZnO matrix.

The tetrahedral sites preferred because of its ability to form covalent bonds.UV-Vis optical absorption spectra of ZnO and ZnNiCaFeO NPs have been recorded in the range 190-900 nm and the obtained absorption spectra is shown in Fig. 5. From the UV-Vis spectra, the absorption peaks are found at 296 and 288 nm for ZnO and ZnNiCaFeO NPs, which is attributed to the photo excitation of electron from valence band to conduction band. Thus, the obtianed absorbances of the above samples are depending on several factors including optical band gap, oxygen deficiency, surface roughness and impurity location. Further, the absorption band edge of the ZnNiCaFeO sample has been blue shifted towards the lower wavelength side due to the quantum confinement. The relationship between the incident photon energy (hυ) and absorption coefficient (α) can be written as

$$\alpha h\upsilon = A(h\upsilon - E_g)^n \qquad (5)$$

The optical band gap (Eg), A is the constant and the exponent n depends on the type of The n= 1/2 for allowed direct transition, 2 for allowed indirect transition 3/2 and 3 for forbidden direct and indirect transitions respectively [13]. Considering direct band transition in ZnO NPs, a plot between $(\alpha h\upsilon)^2$ vs. photon energy ($h\upsilon$) and extrapolating the linear portion of the absorption edge to find the intercept with energy axis is shown in Fig. 6. The band gap increases from 3.90 to 3.92 eV in the doped sample due to the effect of metal ions like Ni, Ca and Fe. The reduction in particle size results in increase of surface/ volume ratio. The surface atom has lower coordination number and atomic interaction, which increases the highest valence band energy and decreases the lowest unoccupied conduction band energy.

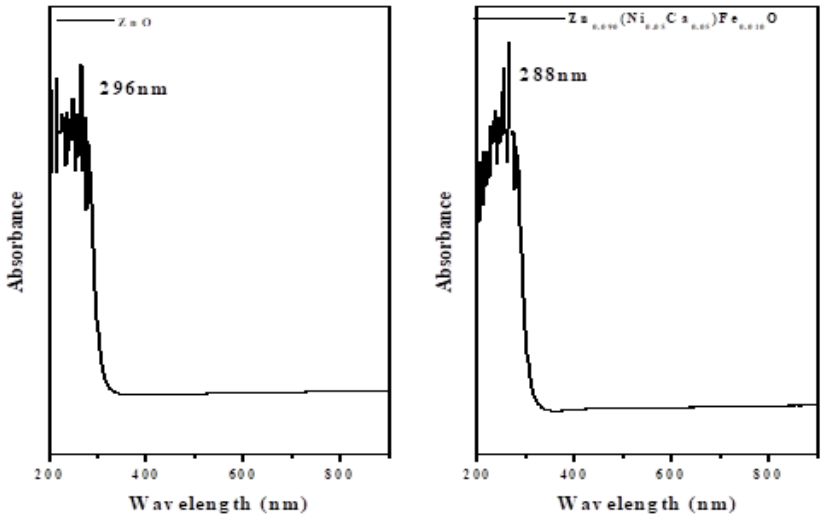

Figure 5. UV-Vis spectra of (a) pure ZnO and (b) ZnNiCaFeO **NPs**

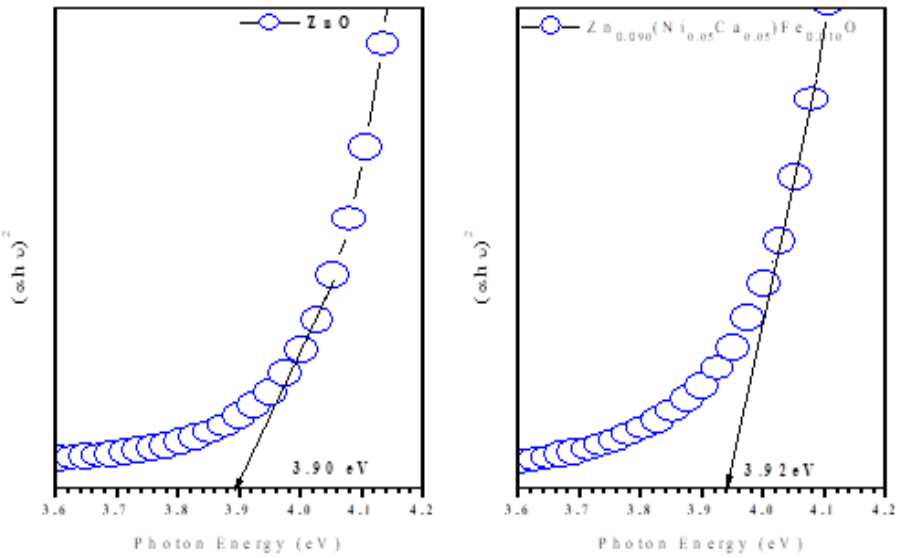

Figure 6: Band gap of (a) pure ZnO and (b) ZnNiCaFeO **NPs**

The Gaussian decomposed photoluminescence emission spectra of the as-synthesized ZnO and ZnNiCaFeO NPs recorded at the excitation wavelength of 350 nm (Fig. 7). The spectra showed a broad emission peaks from 380-580 nm for two samples. Six emission peaks have been obtained from the Gaussian function for the PL spectra of the samples, named as C1-C6 (Table-4).

The emission spectra of the ZnO NPs with six peaks at 386 , 395 , 410 , 459 and 488 nm are shown in Fig. 7(a). The emission spectra observed at 380 and 395 nm range (band to band transition at UV region) are mainly attributed to radiative recombination of the free exciton-exciton collision [14], 412 nm (violet emission) the electron transition from a shallow donor level of the natural zinc interstitials to the top level of the valence band [15], 432 nm (blue emission) ionized Zn vacancies and surface defects in the ZnO NPs[16], 458 and 487 nm (blue-green emission) corresponding to the transition between oxygen vacancy and oxygen interstitial defect vacancies [17-18]. PL emission spectra of ZnNiCaFeO NPs, the red shift has detected and analyzed with ZnO NPs due to various parameters, such as lattice distortion, localization of charge and electron phonon coupling carriers due to interface effects and point defects [19]. A small band shift in the near band edge (387 nm) and violet emission (400 nm), blue emission (438 nm), blue green emission (458 and 498 nm) attributed to the dopant effects (Fig. 7(b)). The yellow emission band is detected at 562 nm in ZnNiCaFeO sample due to the existence of interstitial oxygen vacancies [20]. The shift and variation in the emission values confirmed the presence of Ni, Ca and Fe into the ZnO matrix.

Table 4 Photoluminescence peak position for pure ZnO and ZnNiCaFeO **NPs**

Sample	**Peak position (nm)**					
	C1	C2	C3	C4	C5	C6
ZnO	386	395	410	433	459	488
ZnNiCaFeO	388	400	438	458	498	563

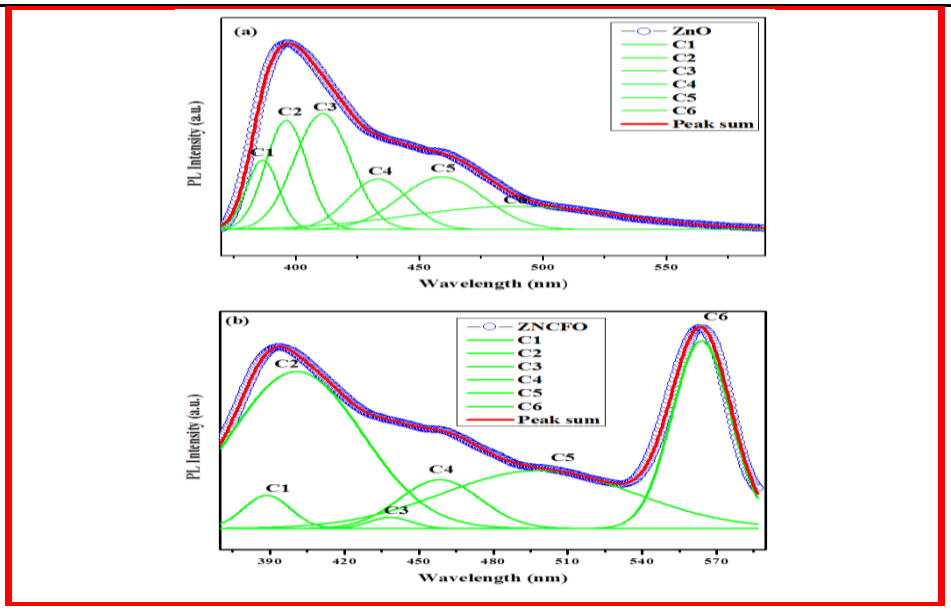

Figure 7 Gaussian de-composed photoluminescence emission spectra of (a) ZnO NPs and (b) ZNCFO NPs

Magnetization versus magnetic field (M-H) curves for ZnO and ZNCFO NPs are shown in Fig. 8. M-H loops were carried out at a temperature of 300 K with maximum applied field ± 20 kOe, to observed the magnetic properties in the combined effect of Ni^{2+}, Ca^{2+} and Fe^{3+}in ZnO matrix. The ZnO NPs exhibits the diamagnetic behavior in this sample [22, 23] and ZNCFO sample exhibit ferromagnetic behavior. The magnetization values of about - 0.02722 emu/g and 0.34914 emu/g were observed at 20 kOe for ZnO and ZNCFO NPs respectively. The result of XRD analysis, the ZNCFO sample, due to the presence of Fe3+ ion, the secondary phase exist.Which is useful to consider all possible ferromagnetic impurity phase present in the sample. Room temperature ferromagnetism is correlated to Fe-related oxide such as Fe_3O_4 or Fe cluster and also the presence of oxygen vacancies will change in the band structure of host semiconductors [24]. In literature, the intrinsic defects play vital role in the ferromagnetism of transition metal doped ZnO and the oxygen vacancies with the trapped occupying an orbital overlapping with the d shells of transition metals [25]. From the results, the PL spectra of ZNCFO and the yellow emission band detected at 562 nm is ascribed to the presence of interstitial oxygen vacancies. The yellow emissions disappear in the sample ZnNiCaFeO NPs as compared to ZNCFO sample. The shift and variation in the emission values confirm the presence of metal Ni, Ca and Fe into the ZnO matrix.

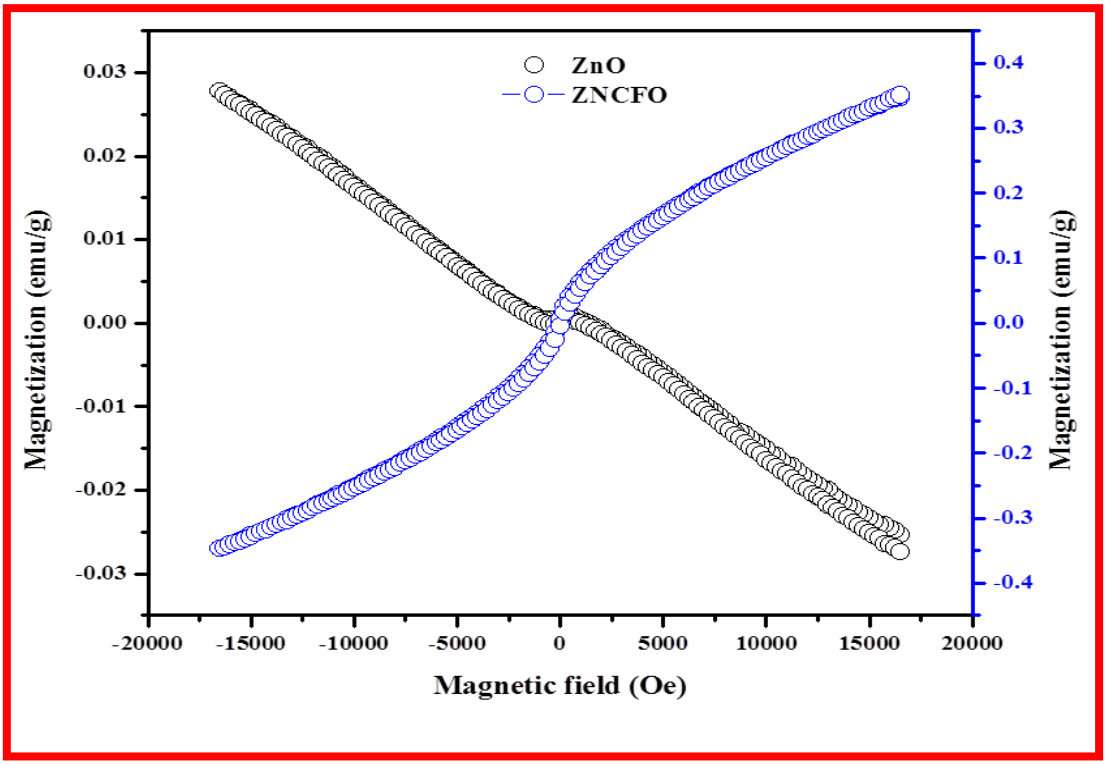

Figure 8 Magnetic hysteries (M-H) curves of the pure ZnO and ZNCFO NPs

Conclusion

Using single step co-precipitation method, the Present study focused on the synthesis of ZnO and ferrite composition ZNCFO.From the XRD patterns, the synthesized ZnO sample and ZNCFO NPs

sample exhibits the hexagonal wurtzite structure.FESEM images showed due to the synthesis ZnO sample and ZNCFO NPs formed hexagonal rod like structures and nanorods filled with uniform grain boundaries.From the EDX analysis, the chemical compositions were estimated. In FT-IR spectral analysis, the several vibrational frequencies were assigned for ZnO and ZNCFO NPs. In the doped sample due to the effect of Ni, Ca, the band gap increases from 3.91 to 3.92 eV.. Room temperature ferromagnetism is correlated to Fe cluster and also the presence of oxygen vacancies in the band structure of host semiconductors.

References

1. Bacaksiz, E., M. Parlak, M. Tomakin, A. Özçelik, M. Karakız, and M. Altunbaş. "The effects of zinc nitrate, zinc acetate and zinc chloride precursors on investigation of structural and optical properties of ZnO thin films." Journal of Alloys and Compounds 466, no. 1-2 (2008): 447-450.
2. Wang, Jun, Jieming Cao, Baoqing Fang, Peng Lu, Shaogao Deng, and Haiyan Wang. "Synthesis and characterization of multipod, flower-like, and shuttle-like ZnO frameworks in ionic liquids." Materials Letters 59, no. 11 (2005): 1405-1408.
3. Xu, Linping, Yan-Ling Hu, Candice Pelligra, Chun-Hu Chen, Lei Jin, Hui Huang, Shanthakumar Sithambaram, Mark Aindow, Raymond Joesten, and Steven L. Suib. "ZnO with different morphologies synthesized by solvothermal methods for enhanced photocatalytic activity." Chemistry of Materials 21, no. 13 (2009): 2875-2885.
4. Cho, S.; Jung, S.-H.; Lee, K.-H. Morphology-Controlled Growth of ZnO Nanostructures Using Microwave Irradiation: From Basic to Complex Structures. J. Phys. Chem. C 2008, 112 (33), 12769–12776.
5. Chantharasupawong, Panit, Reji Philip, Tamio Endo, and Jayan Thomas. "Enhanced optical limiting in nanosized mixed zinc ferrites." Applied Physics Letters 100, no. 22 (2012): 221108.
6. Nair, Swapna S., Jinto Thomas, C. S. Suchand Sandeep, M. R. Anantharaman, and Reji Philip. "An optical limiter based on ferrofluids." Applied Physics Letters 92, no. 17 (2008): 171908.
7. Cetin, Saime Sebnem, Ibrahim Uslu, Arda Aytimur, and Suleyman Ozcelik. "Characterization of Mg doped ZnO nanocrystallites prepared via electrospinning." Ceramics International 38, no. 5 (2012): 4201-4208.
8. Karthikeyan C, Arun L, Hameed AH, Gopinath K, Umaralikahan L, Vijayaprasath G, Malathi P. Structural, optical, thermal and magnetic properties of nickel calcium and nickel iron co-doped ZnO nanoparticles. Journal of Materials Science: Materials in Electronics. 2019 May 15;30(9):8097-104.
9. Chauhan, Ruby, Ashavani Kumar, and R. Pal Chaudhary. "Synthesis and characterization of copper doped ZnO nanoparticles." J. Chem. Pharm. Res 2, no. 4 (2010): 178-183.

10. Fu, Chao-Ming, Ming-Ru Syue, Fu-Jin Wei, Chao-Wen Cheng, and Chan-Shin Chou. "Synthesis of nanocrystalline Ni–Zn ferrites by combustion method with no postannealing route." Journal of Applied Physics 107, no. 9 (2010): 09A519.
11. Hameed, Abdulrahman Syedahamed Haja, Chandrasekaran Karthikeyan, Seemaisamy Sasikumar, Venugopal Senthil Kumar, Subramanian Kumaresan, and Ganesan Ravi. "Impact of alkaline metal ions Mg2+, Ca2+, Sr2+ and Ba2+ on the structural, optical, thermal and antibacterial properties of ZnO nanoparticles prepared by the co-precipitation method." Journal of Materials Chemistry B 1, no. 43 (2013): 5950-5962.
12. Abraham, Nelsa, Alex Rufus, C. Unni, and Daizy Philip. "Nanostructured ZnO with bio-capping for nanofluid and natural dye based solar cell applications." Journal of Materials Science: Materials in Electronics 28, no. 21 (2017): 16527-16539.
13. Xiao, L., Lie, S. H., Hui, Z., Bin, L. B., Trans. Nonferrous Met. Soc. 17 (2007) 814. Zenis, Y. D., Carbon and Ceramic Nanofibres, The Sol-gel Derived Ceramic, Science Mag. Org., 2004.
14. Willander, Magnus, Omer Nur, Jamil Rana Sadaf, Muhammad Israr Qadir, Saima Zaman, Ahmed Zainelabdin, Nargis Bano, and Ijaz Hussain. "Luminescence from zinc oxide nanostructures and polymers and their hybrid devices." Materials 3, no. 4 (2010): 2643-2667. [15] Fan, X. M., J. S. Lian, L. Zhao, and Y. H. Liu. "Single violet luminescence emitted from ZnO films obtained by oxidation of Zn film on quartz glass." Applied surface science 252, no. 2 (2005): 420-424.
15. Mishra, Sheo K., Rajneesh K. Srivastava, S. G. Prakash, Raghvendra S. Yadav, and A. C. Panday. "Photoluminescence and photoconductive characteristics of hydrothermally synthesized ZnO nanoparticles." Opto-Electronics Review 18, no. 4 (2010): 467-473.
16. Heo, Y. W., D. P. Norton, and S. J. Pearton. "Origin of green luminescence in ZnO thin film grown by molecular-beam epitaxy." Journal of Applied Physics 98, no. 7 (2005): 073502.
17. Lin, Bixia, Zhuxi Fu, and Yunbo Jia. "Green luminescent center in undoped zinc oxide films deposited on silicon substrates." Applied physics letters 79, no. 7 (2001): 943-945.
18. Arun, Lija, Chandrasekaran Karthikeyan, Daizy Philip, D. Dhayanithi, N. V. Giridharan, and C. Unni. "Influence of transition metal ion Ni^{2+} on optical, electrical, magnetic and antibacterial properties of phyto-synthesized CuO nanostructure." Optical and Quantum Electronics 50, no. 12 (2018): 414.
19. Liu, Mi, A. H. Kitai, and P. Mascher. "Point defects and luminescence centres in zinc oxide and zinc oxide doped with manganese." Journal of Luminescence 54, no. 1 (1992): 35-42.
20. Noack, Volker, and Alexander Eychmüller. "Annealing of nanometer-sized zinc oxide particles." Chemistry of materials 14, no. 3 (2002): 1411-1417.

21. Zhou, S., Potzger, K., Reuther, H., Kuepper, K., Skorupa, W., Helm, M., Fassbender, J., Journal of Applied Physics, 101 (2007) 09H109.
22. Hong, Nguyen Hoa, Joe Sakai, and Virginie Brizé. "Observation of ferromagnetism at room temperature in ZnO thin films." Journal of Physics: Condensed Matter 19, no. 3 (2007): 036219.
23. Guo, L. W., D. L. Peng, H. Makino, K. Inaba, H. J. Ko, K. Sumiyama, and T. Yao. "Structural and magnetic properties of Mn3O4 films grown on MgO (0 0 1) substrates by plasma-assisted MBE." Journal of magnetism and magnetic materials 213, no. 3 (2000): 321-325.
24. Coey, J. M. D., M. Venkatesan, and C. B. Fitzgerald. "Donor impurity band exchange in dilute ferromagnetic oxides." Nature materials 4, no. 2 (2005): 173.